Reflected Wave Phenomenon in SiC Motor Drives: Consequences, Boundaries, and Mitigation

Balaji Narayanasamy, *Student Member, IEEE*, Arvind Shanmuganathan Sathyanarayanan, Fang Luo, *Senior Member, IEEE*, and Cai Chen, *Member, IEEE*

***Abstract*—In voltage source inverter-based motor drives, the fast switching speeds of the power devices result in the reflected wave phenomenon. Besides the overvoltages at the motor end, there are overcurrents at the inverter end. The overvoltages increase stress on the motor and cable insulation, and the overcurrents affect the power devices. Wide bandgap (WBG) devices have lower switching losses and enable high switching frequencies. However, the reflected wave phenomenon is more pronounced in converters using WBG devices and could potentially increase the switching losses. This article presents a comprehensive analysis of the influence of the reflected wave phenomenon on the switching characteristics of SiC devices in motor drives. Notably, the effect of undamped reflected waves and different cable lengths on both the inverter end and motor end is studied. The analysis and experiments in this article uncover that, depending on the switching instance, the undamped reflected wave causes up to a 30% increase or up to a 15% decrease in the switching losses. A 12% reduction in the switching losses is observed with no cable to up to 20-m long cable. The last part of the article presents the design tradeoffs involved in designing a dv/dt filter. Five different dv/dt filters are compared in terms of their impact on the switching losses, dv/dt at the load, filter loss, and damping time of the reflected wave. The *L* filter and the *RLC* filter have around a 9% reduction in switching losses. The *L* filter suffers from increased damping time and higher reflected wave magnitude, making it unsuitable for high switching frequency applications. Overall, *L* // *R* filter offers the lowest filters losses with a 6% reduction in switching loss, making it more suitable for WBG devices-based high-speed motor drives.**

***Index Terms*—DV/DT filter, motor drives, reflected wave phenomenon, switching losses, wide bandgap (WBG) devices.**

I. Introduction

REFLECTED wave phenomenon in motor drives refers to the overvoltages at the motor end caused by the fast-rising and falling inverter output pulses [1], as shown in Fig. 1. Overcurrents accompany these overvoltages at the motor end [2]. The overvoltages depend on the length of the cable, impedance mismatch between the cable and the motor, the time of application of consecutive pulses, and the damping time of the pulses [3]. The overvoltages increase the insulation stress on the motor and cable [1], and the overcurrents influence the switching characteristics of the devices [2]. Thus, the reflected wave phenomenon affects both the inverter and the motor. Therefore, any method that is used to mitigate the reflected wave phenomenon should take both the inverter switching characteristics and motor overvoltage into consideration. Moreover, the emerging application of SiC wide bandgap (WBG) devices in motor drives with fast switching speeds adds more problems such as undamped reflected waves, thus making the phenomenon even more complicated. Traditional mitigation approaches involve bulky and costly sine wave filters or dv/dt filters, which reduces the benefits of employing WBG devices. Therefore, it is necessary to revisit this phenomenon and incorporate this knowledge in converter design.

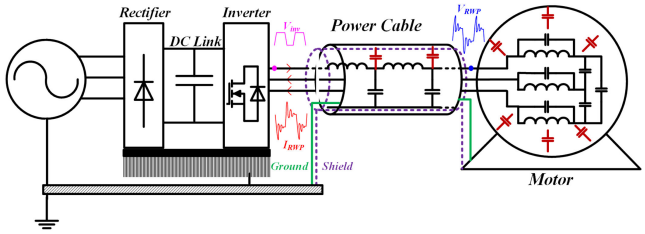

Fig. 1. Typical motor drive.

Previously, various works [4]–[10] have developed design methodologies for various filter topologies to mitigate the overvoltages in Si IGBT-based motor drives. In [11], Swamy *et al.* compared output filter designs for an Si IGBT- and a SiC JFET-based motor drive in terms of filter losses and dv/dt at the motor. Thus, the motor end overvoltage mitigation and filter losses were previously studied in detail. However, the effect of the filters on the switching characteristics has not been studied previously. The study presented in this article fills in the existing gap between the design of filters for overvoltage mitigation and its impact on power device switching performance.

In the wake of emerging applications such as all-electric aircraft, the demand for high power density, high-speed motors, and their drive systems is increasing. Further, these high-speed motors tend to have low winding inductance and thus require high switching frequency motor drives. The high switching speeds and switching frequency capability of SiC devices enables the

Manuscript received December 27, 2018; revised May 14, 2019, August 20, 2019, and November 21, 2019; accepted February 10, 2020. Date of publication February 20, 2020; date of current version June 23, 2020. Recommended for publication by Associate Editor Prof. D. Costinett. *(Corresponding author: Balaji Narayanasamy.)*

Balaji Narayanasamy and Fang Luo are with the Department of Electrical Engineering, University of Arkansas, Fayetteville, AR 72701 USA (e-mail: bnarayan@uark.edu; fangluo@uark.edu).

Arvind Shanmuganathan Sathyanarayanan is with the Ohio State University, Columbus, OH 43210 USA (e-mail: sathyanarayanan.5@osu.edu).

Cai Chen is with the Huazhong University of Science and Technology, Wuhan 430074, China (e-mail: caichen@hust.edu.cn).

Color versions of one or more of the figures in this article are available online at http://ieeexplore.ieee.org.

Digital Object Identifier 10.1109/TPEL.2020.2975217

possibility of high fundamental frequency motor drives. Switching frequencies up to 100 kHz were demonstrated in voltage source inverter-based motor drives using SiC devices [12]. Such high switching frequency brings new concern in the area of reflected wave mitigation. Most of the previous works that analyzed reflected wave phenomenon, utilized Si IGBTs operating at switching frequencies of a few kilohertz. There was sufficient time for the reflected waves to damp out before the next pulse was applied. Hence, there was less concern to investigate the effects of undamped reflected wave on the switching characteristics of devices. But, while switching at tens of kilohertz to lower hundreds of kilohertz, the subsequent pulses could occur before the reflected wave from the previous pulse could die out. Therefore, it is essential to understand the effects of undamped reflected wave voltages on the switching characteristics of the devices. This article studies the effect of undamped reflected wave on the switching characteristics of SiC devices.

Further, due to the intrinsic characteristics of SiC devices, such as small junction capacitance, small specific on-resistance, and high di/dt and dv/dt during fast switching transients, their switching behavior becomes more susceptible to parasitics and noise of the application circuit [13]. With high switching frequencies, even a small increase in switching losses translates into a significant impact on the overall system efficiency. The parasitic capacitance could arise from PCB (in the case of discrete devices), device drain to the heatsink, output cable, and the load [13]–[16]. These parasitic capacitances would increase current overshoot and switching times, thereby increasing switching loss [14]. Previously, in [15], Walder *et al.* used a 5-m cable along with an inductor; in [13], Zhang *et al.* used a 2-m cable along with a 6.5-kW induction motor; and in [16], Yi *et al.* used a 2.44- and 152.4-m cable along with a 112-kW (150 HP) induction motor to study the switching characteristics of SiC devices in a half-bridge configuration in a double pulse test (DPT) setup. Both Walder *et al.* and Zhang *et al.* [17] and [15], propose utilizing an inductor at the output to reduce switching losses due to the cable and the motor loads. However, the impact of the output inductor on the motor end voltage or the damping time of the reflected wave was not studied. Also, the influence of different cable lengths on the switching characteristics was not studied. Besides, in previous works, the test setup does not include connecting the case of the motor and the heatsink to the ground, which would be the case in an actual motor drive system. This article uses a test setup that resembles an actual motor drive system and studies the effect of output inductors and other different filters on both the inverter switching characteristics and motor overvoltages. Some of the preliminary results were reported in [18] and[19].

There are three significant contributions in this article. First, the effect of undamped reflected waves on the switching characteristics of the devices, and the motor voltages is studied. Second, the effect of different length of the cable on both the switching characteristics and the motor voltages is studied. Finally, the effect of different filters on the inverter end along with the losses in the filter is studied.

The rest of this article is organized follows. Section II describes the effects of the undamped reflected waves, length of the cable, and filters on the device switching characteristics. Section III describes the experimental test setup used in this work. Section IV discusses the experimental results that detail the influence of undamped reflected waves on the switching characteristics and reflected wave phenomenon. Section V discusses the experimental results involving the impact of length of the cable on the device switching characteristics and reflected wave phenomenon. In Section VI, five different topologies of filters that have been used to mitigate reflected wave phenomenon are designed and tested. The filters are compared in terms of the switching loss reduction, filter losses, and dv/dt at the motor.

II. Effects of Reflected Wave Phenomenon on Switching Characteristics

In a motor drive system, the interconnecting cable behaves like a transmission line. The characteristic impedance (Z_c) of the power cables is in the range of 48 and 150 Ω [20]. The motor load tends to have high impedance (Z_L) than that of the power cable. Due to this impedance mismatch, when a pulse is applied at one end of the inverter, reflections occur at the motor end. According to theory on reflections [7], [21], when a pulse of voltage is applied to the combination of the cable and the motor, a pulse of current travels along with it. This voltage pulse upon reaching the motor is reflected along with the motor current. This voltage and current once again undergo reflections at the source end. The magnitude of the reflected current and voltage depends on the nature of the impedance that reflects them. For a given load, the theoretical peak reflections occur only if the rise (fall) times are lower than two times the propagation time of the cable. Reflections occur both during turn ON and turn OFF of the device. Therefore, it becomes necessary to understand the impact of the reflected waves on the switching characteristics of the devices. The impact of the undamped reflected wave, length of the cables, and output filters on the switching characteristics of the power devices is discussed below.

A. Effect of Undamped Reflected Waves

Undamped reflected wave (RW) could result in RW voltages higher than 2 pu. Different control methods [22], [23] have been proposed to avoid double pulsing for switching frequencies up to 20 kHz [23]. But, at higher switching frequencies, the impact of the undamped RW is even higher. The frequency of oscillation of the reflected wave mainly depends upon the frequency of first antiresonance in the impedance of the motor and the length of the interconnecting cable [1]. In motors, the frequency at which the first antiresonance occurs reduces with the power level. This is shown by measuring the differential mode impedance of the motors of different power levels. The measurement configuration is shown in Fig. 2(a). Three induction motors of power level 2 kW (Toshiba), 15 kW (Baldor), and 150 kW (Baldor) are measured and shown in Fig. 2(b). The first antiresonance occurs at frequencies of 16, 8, and 3.2 MHz for 2-, 15-, and 150-kW motors, respectively. Therefore, for a given length of the cable, the frequency of the reflected wave is different for different power levels. Further, for a given power level, the frequency of reflected wave reduces with the increase in the

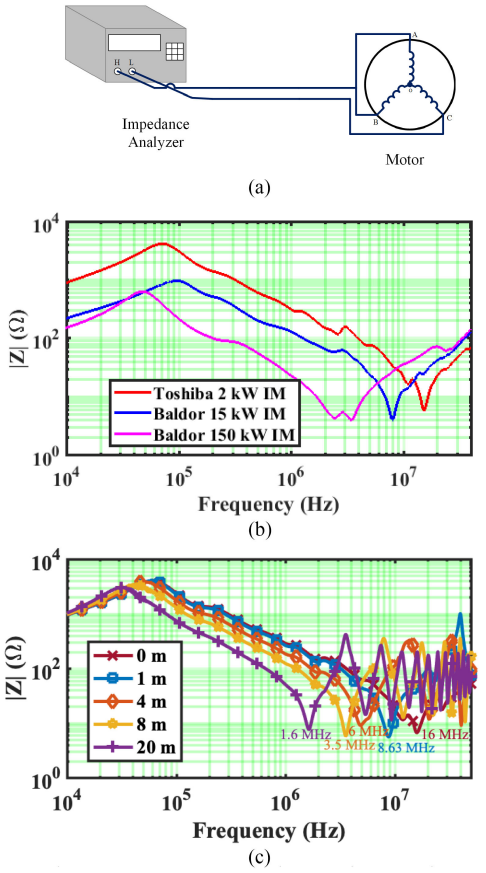

Fig. 2. (a) Schematic of measurement. (b) Impedance of different induction motors. (c) Impedance of 2-kW induction motor with different cable lengths.

length of the cable. The impedance of a Toshiba 2-kW induction motor connected to Lapp 700700 2-kV 16 AWG power cable at different cable lengths is shown in Fig. 2(c). With increasing length, the frequency of the first antiresonance shifts to lower and lower frequencies. The frequency of the first antiresonance reduces from 16.1 MHz with no cable to 8.6, 5, 3.5, and 1.6 MHz as the length of the cable is gradually increased from 1, 4, 8, and 20 m, respectively. The frequency of the reflected wave determines the damping time.

The factors that contribute toward the damping time (t_d) of the reflected wave are the ac skin resistance of the motor and cable, and proximity effect in the cables. Therefore, for a given l_c and Z_L, t_d is higher for higher power load and motor. This is because of lower skin resistance with increasing cable and motor winding thickness. The time to damp the reflected pulses to 5% of the initial peak value is given as [1]

$$e/e_o = \epsilon^{-r_s l_c/2Z_o} = \epsilon^{-t/\tau}. \tag{1}$$

The 3τ damping times for different cables and at different frequencies are shown in Fig. 3(b). The damping time ranges from a few microsecond to tens of microsecond for a reflected wave frequency of 1 MHz at different cable sizes. This becomes an important consideration with ever-increasing switching frequencies for inverters. When the next pulse is applied before the reflected wave due to the previous pulse is damped, the

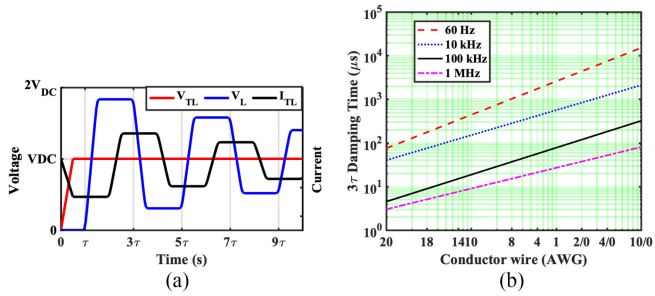

Fig. 3. (a) Reflected wave voltage and current progression. (b) 3τ damping time at different frequency and different cable AWG for length of 30 m.

current through the device during the switching action changes drastically. The next pulse can be applied during the peak, trough, or middle of the reflected wave.

When a pulse voltage is applied, reflected wave currents and voltages occur, as shown in Fig. 3(a). When the device turns OFF, the reflected wave currents freewheel through the top diode. Now, when the device turns ON again, the reflected wave currents transfer from the diode to the device. Depending on the instance at which the device turns ON, higher or lower than normal currents could flow through the device. This drastically changes the switching losses in the devices. The next pulse can be applied during 1τ–3τ time of the reflected wave.

This effect is more prominent in higher power level motor drives with longer cable lengths. The longer the length of the cable, the lower is the frequency of the reflected wave. At higher power levels, the ac resistance due to skin effect is lower, and therefore this effect is more pronounced.

B. *Effect of Cable Lengths*

The inductance and capacitance of the cable in differential mode configuration for 1-m cable length are denoted as L_C and C_C, respectively. The length of the cable and the time of propagation of the reflected wave per meter is denoted by l_C and t_p, respectively. The cable characteristic impedance, load side reflection coefficient (Γ_L), and peak magnitude of the overvoltages are given in (2), (3), and (5). The frequency of the reflected wave is ideally given by (5). However, when the antiresonance of the cable is close to the motor's antiresonance, then the frequency is dominated by the motor's impedance [24]

$$Z_C = \sqrt{\frac{L_C}{C_C}} \tag{2}$$

$$\Gamma_L = \frac{Z_M - Z_C}{Z_M + Z_C} \tag{3}$$

$$V_{\text{load}} = (1 + \Gamma_L)V_{dc} \tag{4}$$

$$f_{\text{RW}} = \frac{1}{4l_C t_p}. \tag{5}$$

According to the theory on reflections [7], [21], the repeated reflections could be approximated in the form of a decaying sine wave. The frequency of the reflected wave voltages and currents depends upon the time taken for propagation through the cable.

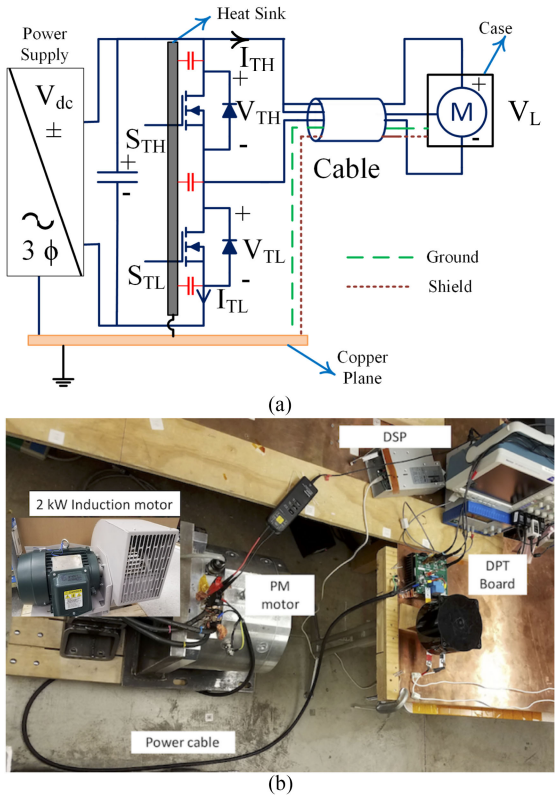

Fig. 4. (a) Schematic of test setup. (b) Laboratory test setup (insert shows the 2-kW induction motor).

One complete cycle of reflected wave consists of two reflections (one at the source side and the other at load side). Therefore, the reflected wave has a period equal to 4 times the propagation time of the reflected wave. While this holds for cable lengths higher than a few tens of meters, short cable lengths are affected differently. At shorter cable lengths, the motor's antiresonance dominates [24], and therefore the conventional explanation for the frequency of reflected wave does not hold good.

That said, the majority of the HF currents occur at first antiresonant frequency which corresponds to the frequency of the reflected wave. And, therefore, the rest of high-frequency antiresonances have a lesser impact on the switching losses of devices. Therefore, if the frequency corresponding to the switching speed of the device is lower than the antiresonance frequency, then the reflected wave currents cause an increase in the current flow through the device during the switching action. This causes switching losses to increase. For a given switching speed, an increase in cable length reduces the frequency of the reflected wave voltages and currents. Therefore, the reflected wave currents that flow through the device during switching transients are lowered, leading to lower switching losses.

C. Effect of Output Filters

One of the key purposes of using the filter is to damp the RW voltages. While each filter could be designed to provide the same magnitude of RW voltage, other metrics vary. The dv/dt reduction is a key factor here since it increases the bearing currents in the motor. The undamped RW could increase the switching losses of the device, and therefore, the RW damping time also needs to be taken into consideration. On top of this, the filter could help trim the high-frequency impedance seen by the SiC devices, thus reducing the switching losses. The impact of different output filters used to mitigate the reflected wave phenomenon and its effect on the switching characteristics is studied. The impact of the filters on the switching characteristics is identified from their interaction with motor and cable impedance. Five commonly used filters are designed and compared in terms of the losses in the filter and reduction in switching losses. The five filters include, the output inductor, *RC* [7], *RLC* [6], *LR* [5], and *L* // *RC* (*L* parallel *RC*) [9].

TABLE I
CONSTITUENTS OF TEST SETUP

DPT Board	Wolfspeed KIT8020CRD8FF1217P-1
Device	Wolfspeed C2M0080120D
Anti-parallel Diode	Wolfspeed C4D20120D
Cable	Lapp 700700 - 4 Core 16 AWG 2 kV Shielded Cable
Motor	2 kW Induction Motor and 100 kW PM motor

TABLE II
MEASUREMENT INSTRUMENTS

Oscilloscope	Tektronix MSO-58 8 channel 2 GHz
V_{TL},V_{TH} and V_L	Tektronix THDP0200 200 MHz Differential Probe
I_{TL}	T&M Research SSDN-10 1 GHz current shunt
V_{TL}	Tektronix TCP0030A 120 MHz current probe

III. EXPERIMENTAL TEST SETUP

The schematic of the test setup is shown in Fig. 4(a) and the test setup is as shown in Fig. 4(b). The constituents of the DPT are listed in Table I. A CREE SiC half-bridge evaluation board [25] is used to realize the DPT circuit. The lower device of the half-bridge is under study here. The DPT test setup is configured to measure bottom device current (I_{TL}) and voltage (V_{TL}), top device voltage (V_{TH}), cable current at the inverter end (I_{TH}), and motor voltage (V_L). The oscilloscope and probes used for measurement are listed in Table II. The motor is supplied using a 16 AWG 2-kV Lapp 700700 VFD cable [26], and the test condition is 600 V and 10 A. For studying the effects of damping time and length of cable, a 2-kW induction motor is used and for filter designs, a 100-kW PM motor is used. The effect of filters depends only on the interaction of the filter impedance and the motor impedance and therefore is acceptable to use the 100-kW PM motor. As will be shown in the later sections, the magnitude of the peak RW with a 4-m cable is almost the same with both the motors.

In order to evaluate the influence of the different phenomenon, it is essential to have a standardized test setup. The test setup is configured to represent a single switching state of the voltage source inverters (VSI) under operation. Two of the three-phase cables are connected to the positive of the dc link, and the third phase cable is connected to the midpoint of the half-bridge. At the other end, the three cables are connected to three-phase terminals of the motor. To represent the actual condition of a motor drive system, the SiC half-bridge board is placed on a copper plane (which mimics

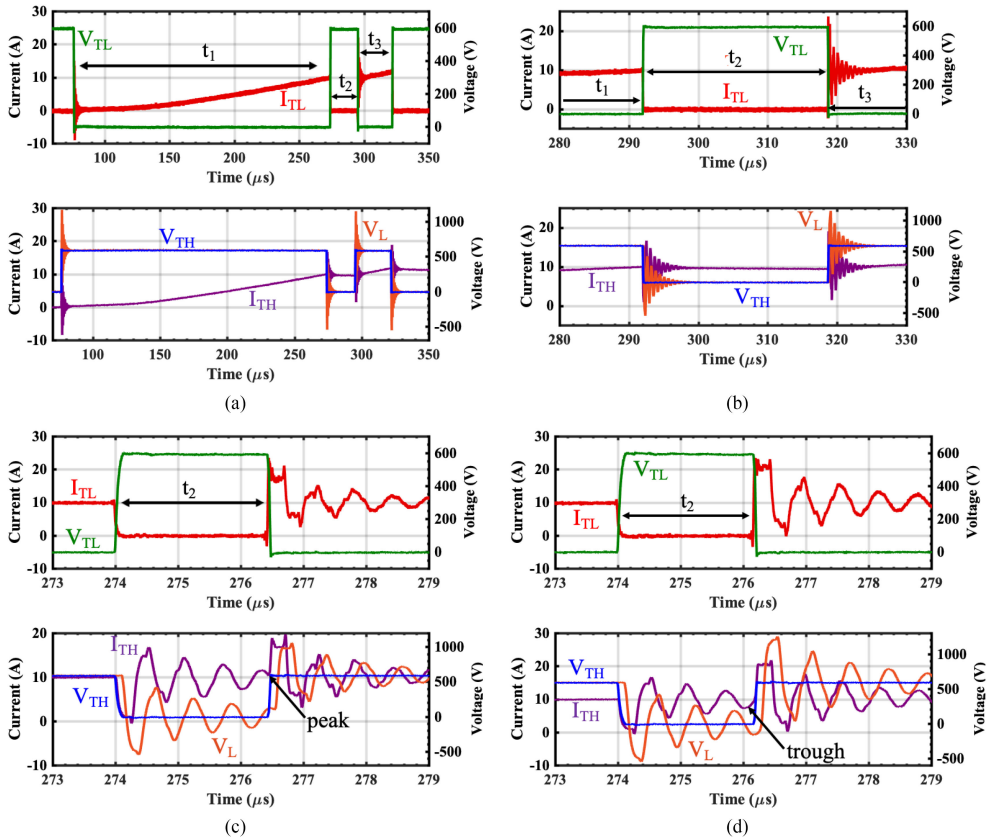

Fig. 5. (a) Timings of pulses in a typical DPT. (b) t_2 sufficient for the reflected wave to damp. (c) t_2 insufficient for reflected wave to damp and switching ON of bottom device at peak of reflected wave current (undamped case-2). (d) t_2 insufficient for reflected wave to dam switching ON of bottom device at trough of reflected wave current (undamped case-1).

the drive cabinet), and the heatsink is also connected to it. The ground and shield conductors of the cable are connected to the copper plane on the device side and to the case of the motor on the other end. In motor drive systems, this is done to provide a path for the CM noise to return back to the inverter. It is essential to connect the copper plane to the power earth to which the dc power supply's ground is also connected.

IV. Influence of Undamped Reflected Wave on Switching Characteristics

The phenomenon will be explained using the 2-kW inverter and 20-m cable. As stated earlier, the effect of this phenomenon is more pronounced in high power drives. However, the illustration here is limited by the equipment available. Let t_1, t_2, and t_3 be the period of the pulse corresponding to first turn ON, turn OFF, and second turn ON of the bottom device, respectively. Experimental measurements from the DPT with the timings marked are shown in Fig. 5(a). Time t_1 is selected such that the required current is reached at the given dc-link voltage. Time t_3 is selected such that it is at least higher than the device turn-ON time. During time t_2, the current freewheels through the antiparallel diode and body diode of the top device. In a conventional DPT, t_2 is set such that there is sufficient time for the device to turn OFF but not high enough that the freewheeling current decays to a lower value. However, when using a cable and motor in the DPT test setup, the minimum time should be set by taking another factor into account. If t_2 is set such that the ringing in the current does not die out before the bottom device turns OFF (start of t_3), this current will cause an increase or decrease in the switching losses depending on its magnitude. This is particularly critical when testing with longer cable lengths. Since, for given gauge of cable, the damping times also increase with increase in cable length [27].

The switching transients and motor voltage for the case where t_2 is large enough for the reflected waves to damp are shown in Fig. 5(b). Now, t_2 is lowered to 2 μs such that the reflected wave due to the previous pulse does not dampen out. There are two subcases—when I_{TH} is, near one of its peak (undamped case 2), and near one of its troughs (undamped case 1). The corresponding measurements are shown in Fig. 5(c) and (d), respectively.

The switching transients during turn ON and turn OFF of the bottom device that includes V_{TL}, I_{TL}, V_{TH}, I_{TH}, and V_L for all the three cases are shown in Fig. 6. The two undamped cases would be compared to the damped case in terms of switching losses. From Fig. 6(a), it could be observed that the undamped case 2 (near peak) has higher current flowing through the bottom device during switching than the damped case. This results in an increase in the switching loss during the ON-transient. For

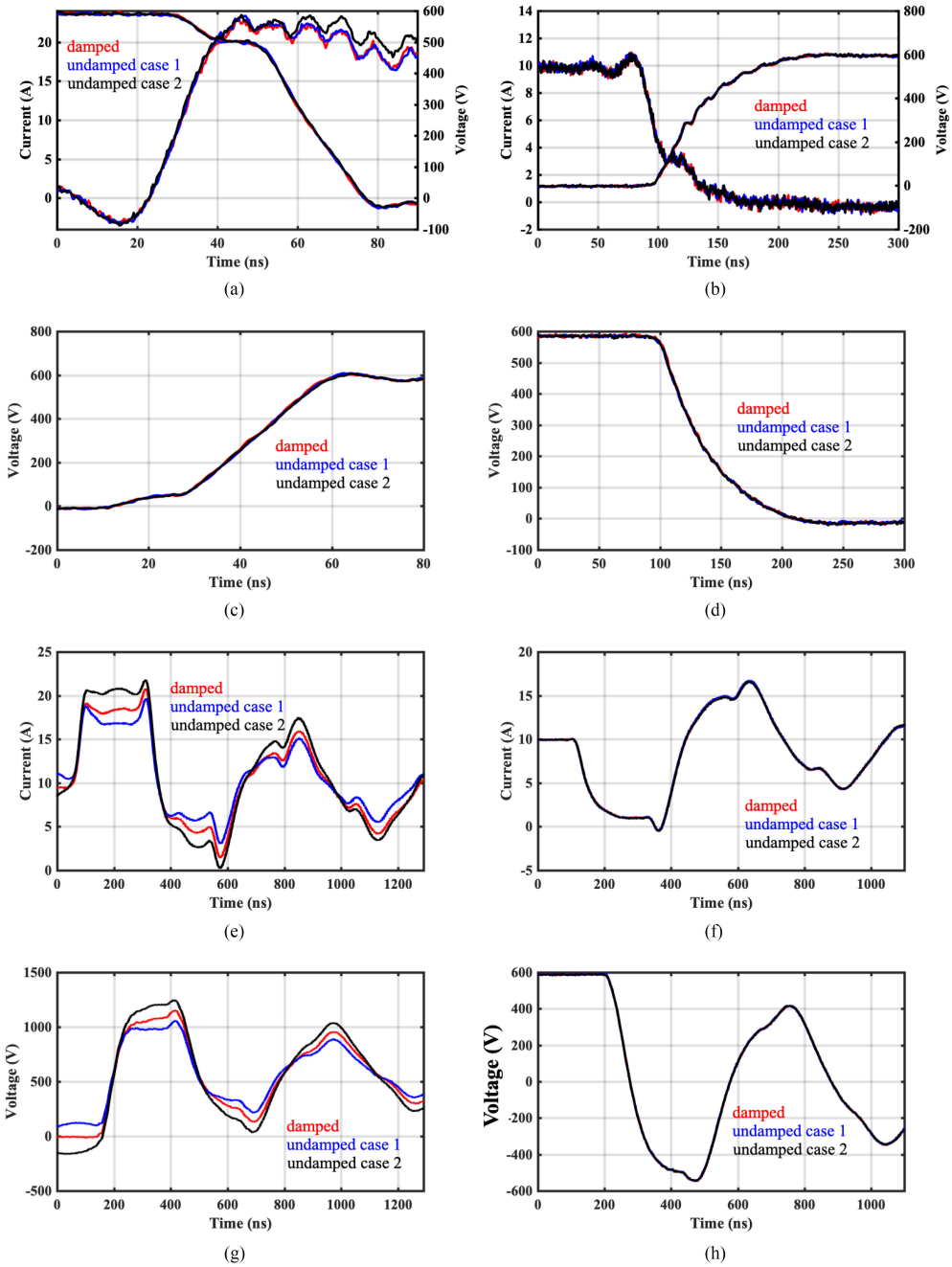

Fig. 6. Effect of undamped reflected wave voltages on the switching characteristics and peak load voltage. (a) ON-transient: V_{TL} & I_{TL}. (b) OFF-transient: V_{TL} & I_{TL}. (c) ON-transient: V_{TH}. (d) OFF-transient: V_{TH}. (e) ON-transient: I_{TH}. (f) OFF-transient: I_{TH}. (g) ON-transient: V_L. (h) OFF-transient: V_L.

the undamped case 2 (near peak), the current increases and for the undamped case 1 (near trough), the current decreases when compared to the damped cases. The peak overvoltage at the motor end V_L also increases for the undamped case 2 (near peak) and reduces for the undamped case 1 (near trough). During the OFF-transient, the reflected wave is completely damped out and therefore, the turn-OFF losses E_{off} and the switching transients are identical in all the cases.

The tests are repeated for different times, such that the switching action takes place near the different peaks and troughs of the reflected wave current. The results of the experiments are summarized in Table III. The changes in E_{on} and the peak V_L are plotted in Fig. 7(a) and (b). The worst-case turn-ON loss for the undamped case 2, E_{on} is 100 μJ or 40% higher than the damped case. This results in the switching loss increase by approximately 30%. The worst case reduction in turn-ON loss is about 53 μJ or 20%. This, in turn, results in the switching loss decrease by approximately 15%. The V_{TL} and V_{TH} are unaffected by this phenomenon. However, the change in currents can be clearly seen in I_{TH}. The maximum change in switching losses and the peak load voltage occur during the 1τ of the reflected wave current. As the reflected wave current dies out,

TABLE III
EFFECT OF UNDAMPED REFLECTED WAVE VOLTAGES

Test Condition	t_2 (μs)	E_{on} (μJ)	E_{off} (μJ)	E_{sw} (μJ)	V_{Load} (V)
RW damps out	4 μ	253	67	320	1150
undamped case-2	2.9 μ	280	67	347	1240
undamped case-1	2.7	200	67	267	1056
undamped case-1	2.2	210	65	275	1234
undamped case-2	1.9	312	68	380	1098
undamped case-2	1.6	303	67	370	1223
undamped case-1	1.4	215	68	283	1229
undamped case-1	1.16	205	67	272	1175
undamped case-2	0.87	352	66	418	1328

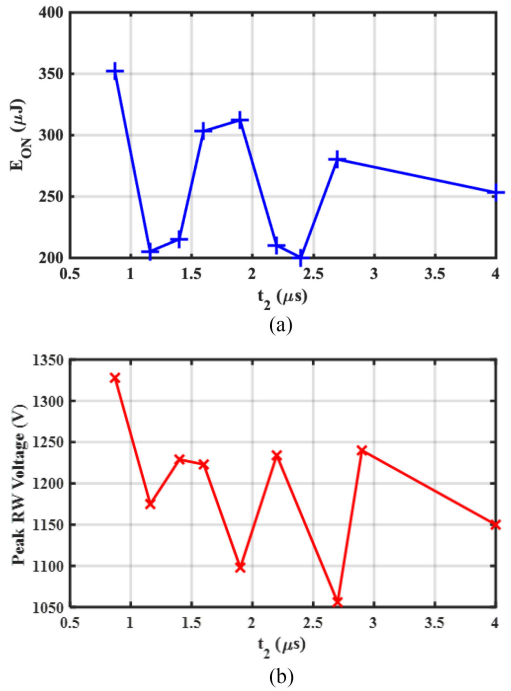

Fig. 7. Turn-ON loss and reflected wave voltage at different value of t_2. (a) E_{on} at different t_2. (b) Peak V_L at different t_2.

the change in E_{on} and V_L slowly die out. Since the reflected wave current starts with a peak value, it would result in a net increase in the switching losses during the continuous operation of the converter. The time period t_2 discussed here is of the order of a few microsecond. This just serves to illustrate the phenomenon. In high power drives, the change in E_{on} and V_L would be much worse due to increased damping times and lower frequency of reflected wave.

The effects of undamped RW on switching losses is illustrated using two examples here which are summarized in Table IV. First one uses MOSFET C2M0080120D from Wolfspeed. The conduction losses are calculated for an average drain current of I_D of 10 A. From the datasheet, $R_{\mathrm{DS}on}$ is 80 mΩ, and thermal resistance from junction to ambient, $R_{\theta\,\mathrm{JA}}$ is 1 °C/W (from datasheet thermal resistance from junction to case, $R_{\theta\,\mathrm{JC}} =$ 0.6 °C/W and assumed thermal resistance from case to ambient

TABLE IV
TEMPERATURE RISE DUE TO UNDAMPED REFLECTED WAVE VOLTAGES FOR f_{sw} OF 100 kHz

Case	C2M0080120D			CAS325M12HM2		
	E_{sw} (μJ)	P_{sw} (W)	T_j (^oC)	E_{sw} (mJ)	P_{sw} (W)	T_j (^oC)
RW damped	320	32	137	8	800	148
RW undamped-1	418	41.8	146.8	10	1000	172
RW undamped-2	267	26.7	131.7	6.7	670	133

$R_{\theta\,\mathrm{CA}} = 0.4$ °C/W) and an ambient temperature T_A of 25 °C is considered here. Conduction loss, P_C is I_D^2 $R_{\mathrm{DS}on}$ is equal to 80 W. The E_{sw} ($E_{on} + E_{off}$) is taken from the measurement and is used to calculate the switching losses at different switching frequencies. Three cases are considered here (RW completely damped, undamped peak, and undamped trough). Switching loss, $P_{\mathrm{sw}} = f_{\mathrm{sw}}$ E_{sw} and P_{tot} is the sum of P_C and P_{sw} and device junction temperature is given by

$$T_j = R_{\theta\,\mathrm{JA}}\, P_{\mathrm{tot}} + T_A. \tag{6}$$

As mentioned previously, the undamped RW is major concern for high speed motor drives which require switching frequencies up to a few hundred kilohertz. Therefore, calculations are carried for f_{sw} of 100 and 200 kHz for illustration. For f_{sw} of 100 kHz, the junction temperature of the discrete device changes by about 9.8 °C, which is not very significant. However, the junction temperature changes are much more significant in case of a power module - Wolfspeed CAS325M12HM2 (1.2 kV, 300 A, 3.7 mΩ module). The switching losses from the datasheet are adjusted by the same amount for the undamped case as obtained from the experiment. For calculations, the thermal resistance from junction to ambient, $R_{\theta\,\mathrm{JA}}$ is 0.12 °C/W (from datasheet, the thermal resistance from junction to case, $R_{\theta\,\mathrm{JC}} = 0.1$ °C/W and assumption of thermal resistance from case to ambient $R_{\theta\,\mathrm{CA}} = 0.02$ °C/W) and an ambient temperature T_A of 25 °C is considered. Conduction losses for an average of current of 250 A is 231 W. For f_{sw} of 100 kHz, the junction temperature changes by 15–24 °C for undamped RW. Thus the undamped RW can have significant impact on junction temperature at higher power levels. However, other factors such as dead time, in addition to the switching frequency and cable length, also need to be taken into account in order to gauge the overall impact of undamped RW on the switching losses. Owing to the limitation of space, this analysis will be part of future publication.

V. INFLUENCE OF CABLE LENGTH ON SWITCHING CHARACTERISTICS

This section studies the effect of different lengths of cable along with a motor on the influence of switching characteristics. The phenomenon discussed previously is verified experimentally. The tests are carried out using the motor only (no cable) and with 1-, 2-, 3-, 4-, 5-, and 20-m lengths of cable. The tests are carried out with gate resistors of R_{on} of 5 Ω and R_{off} of 10 Ω, respectively. The experimental results showing the switching transients are shown in Fig. 10 and the results are summarized in Table V. The impedance of the motor connected with different

TABLE V
INFLUENCE OF CABLE LENGTH ON SWITCHING CHARACTERISTICS
($R_{on} = 5\,\Omega$ $R_{off} = 10\,\Omega$)

Cable length (m)	T_{On} (ns)	T_{Off} (ns)	E_{On} (μJ)	E_{Off} (μJ)	E_{sw} (μJ)	$V_{Load-peak}$ (pu)
0	47	82	307	66	373	743
1	47	83	281	67	348	793
2	46	84	276	66	342	980
3	46	88	270	65	335	1024
4	46	94	269	59	328	1067
5	46	94	265	58	323	1098
20	45	96	252	60	313	1163

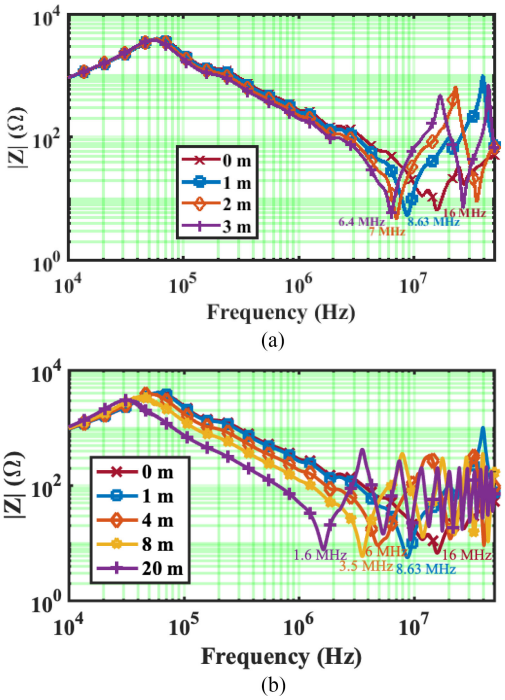

Fig. 8. Impedance of cable + motor with different cable length. (a) 0–3 m. (b) 0–20 m.

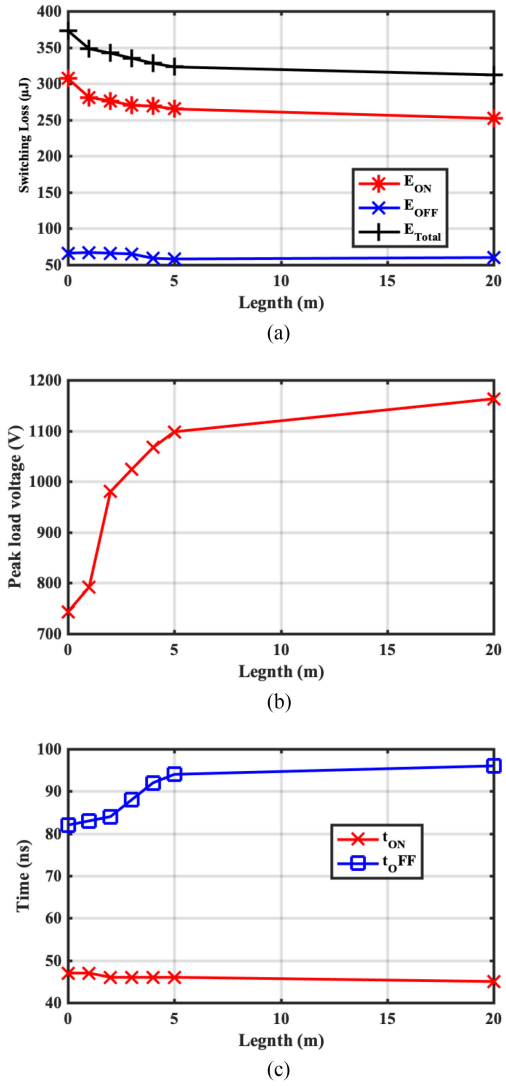

Fig. 9. Effect of different cable lengths on switching characteristics and reflected wave phenomenon. (a) Length of cable versus T_{on} and T_{off}. (b) Length of cable versus peak V_L. (c) Length of cable versus t_{on} and t_{off}.

lengths of the cable is given in Fig. 8. From Fig. 8, without cable, the first antiresonance occurs around the frequency of 16.1 MHz. With an increase in cable length, this resonance point starts shifting further to lower frequencies and more antiresonances occur at higher frequencies. For cable lengths of 1, 2, 3, 4, and 20 m, the first antiresonance occurs at 8.63, 7, 5.4, 5, and 1.6 MHz, respectively. The magnitude of the reflected wave voltages increases with the increase in cable lengths. For lengths of 1 and 2 m, full reflections do not occur because the propagation time is lower than the rise time of the pulse during the ON-transient. Also, during the OFF-transient, the magnitude of the reflections is lower for 1-, 2-, 3-, and 4-m cables because the fall time of the pulse is lower than the propagation time.

The variation of switching losses (E_{on}, E_{off}, and E_{sw}), peak reflected wave voltage (V_L), the switching times (t_{on} and t_{off}) with the length of the cable, and are plotted in Fig. 9. The switching losses can be seen to decrease with an increase in cable length. For 5-Ω gate resistance, the frequency corresponding to the turn-ON voltage transient is 6.7 MHz. The turn-ON losses are highest for the no cable and gradually reduce with an increase in cable length. Since the majority of turn-ON losses come during the current fall transient, it is not affected by the changing cable lengths. The reduction in switching losses is about 16%. The turn-ON times also reduces with increase in the cable length from 47 to 45 ns. But, the decay of the OFF-transient current is affected by the cable length, and therefore the switching time increases from 82 to 96 ns, which corresponds to a 17% increase in switching time. Also, the reflected wave voltages increase steadily from no cable to 4 m from 743 to 1163 V.

VI. INFLUENCE OF OUTPUT FILTERS ON SWITCHING CHARACTERISTICS

As previously mentioned in Section II, the interaction of filter impedance with the impedance of the cable and motor will be used to explain the influence of the filters on the switching

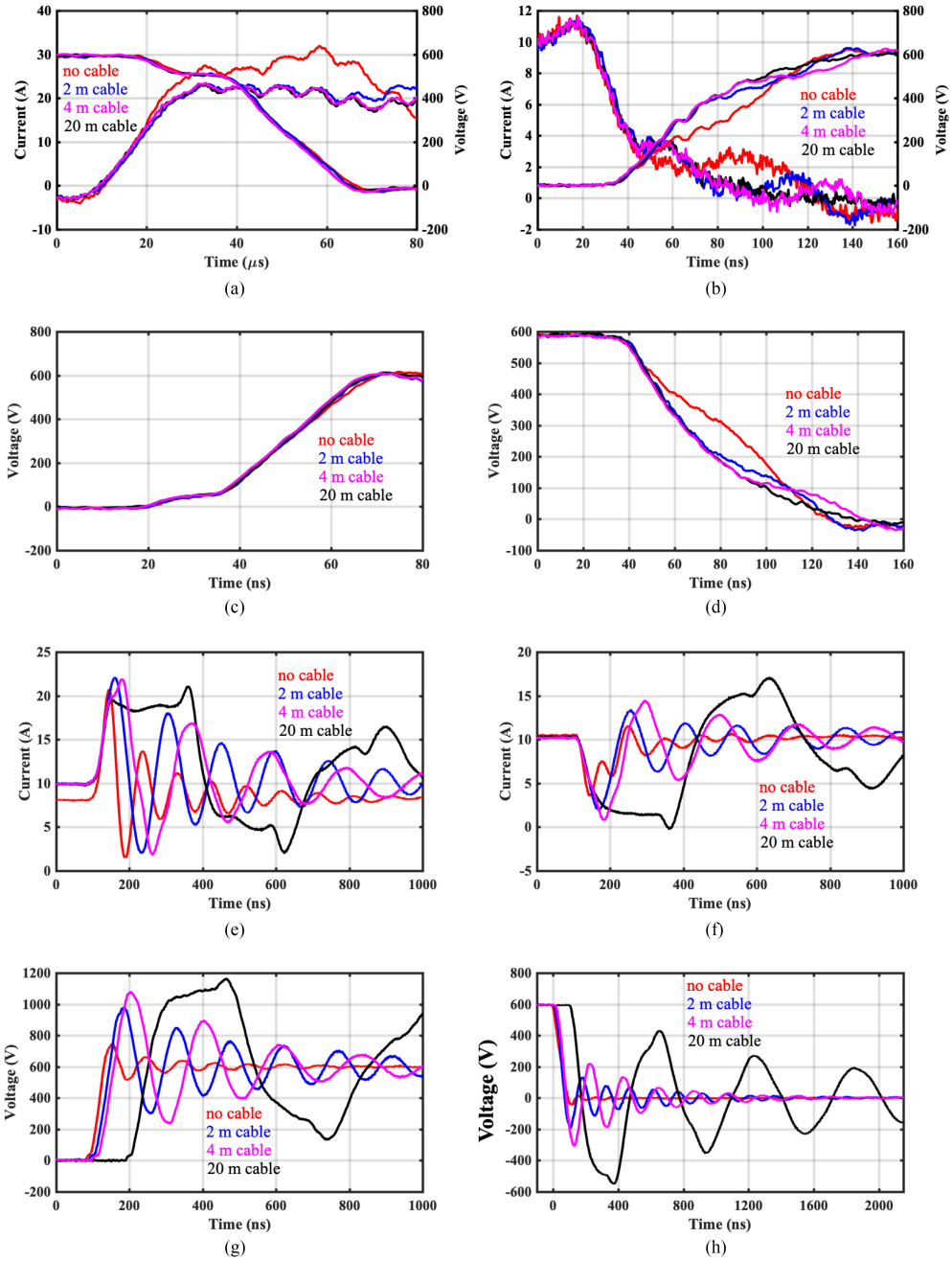

Fig. 10. Switching transients with different cable lengths. (a) ON-transient: V_{TL} & I_{TL}. (b) OFF-transient: V_{TL} & I_{TL}. (c) ON-transient: V_{TH}. (d) OFF-transient: V_{TH}. (e) ON-transient: I_{TH}. (f) OFF-transient: I_{TH}. (g) ON-transient: V_L. (h) OFF-transient: V_L.

characteristics and therefore is not dependent upon the type of motor used. From Figs. 10(e) and 13(c), the peak magnitude of the reflected wave without any filter when a 4-m cable is used is about 1060 V for both the 2-kW induction motor and the 100-kW PM machine. All the filters are designed such that the reflected wave voltage at the motor is reduced from 1.7 pu without the filter to less than 1.2 pu with the filters. The key purpose of using the filter at inverter output is to damp the RW voltages. While different filter topologies could be designed to provide the same magnitude of RW voltage, other metrics such as the dv/dt, filter losses, and damping time vary. The dv/dt reduction is a key factor here since it is related to the bearing currents in the motor. Also, the undamped RW could increase the switching losses of the device and therefore, the RW damping time also needs to be taken into consideration for filter design. On top of this, the filter could help trim the high-frequency impedance seen by the SiC devices, thus reducing the switching losses. The filters are designed for a specific case of 4-m cable length and for a 100-kW PM motor. The gate resistance of 5 Ω is used for both turn ON and OFF. Previously, an output inductor was proposed in [15] and [17] to reduce the switching losses. In this section, the output inductor compared with other filters such as *RC* [7],

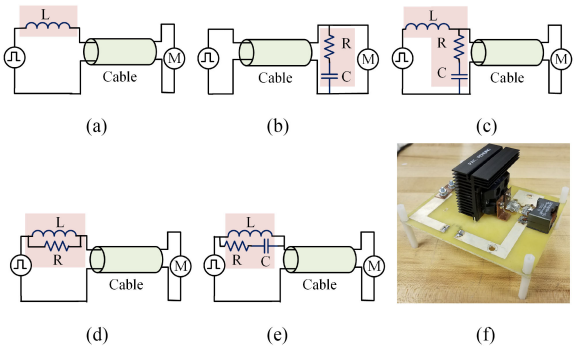

Fig. 11. Different filters and one of the prototypes of filter. (a) L_{aux} filter. (b) *RC* filter. (c) *RLC* filter. (d) *LR* filter. (e) *L* // *RC* filter. (f) Filter prototype.

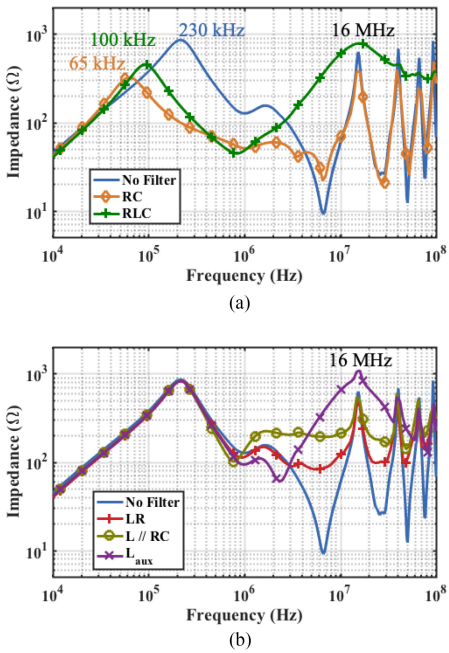

Fig. 12. Impedance with different cable lengths and filters. (a) Measured Impedance of motor, 4-m cable and filters. (b) Measured impedance of motor, 4-m cable and filters.

RLC [6], *LR* [5], and *L* // *RC* (*L* parallel *RC*) [9]. Simplified schematic of the filters and PCB prototype of one of the filters is shown in Fig. 11.

Since only the device switching losses are considered here, the losses in the filter are also calculated during the switching transients so that they could be scaled up to any switching frequency. During the switching transients, the losses in the resistors of the different filters are dominant when compared to that of the losses in the inductor and capacitor. The currents and voltages through the resistors and their product is integrated over the switching interval to calculate the filter losses. Since the inductor values for the *L*, *RLC*, *LR*, and *L* // *RC* are in a similar range, the steady-state core losses and copper losses would be similar and are ignored for simplicity. The component values of inductors, capacitors, and resistors that form the filter are listed in Table VI. The design, the resulting impedance, and the performance of each filter are discussed below.

TABLE VI
FILTER COMPONENTS

Filter	L (μH)	R (Ω)	C (nF)
L[17]	6.8	-	-
RC [7]	-	100	10
RLC [6]	6.8	100	4.7
LR [5]	6.8	100	-
L // RC [9]	15	200	1

The different filters are compared in terms of the losses in the filters, change in the switching losses, switching time, damping time (5% of steady-state value), and dv/dt at the load. The resistors used in the filters are low inductive type from Ohmite [28]. Surface mount inductors from Coilcraft [29] with self-resonant frequencies above 20 MHz are chosen. And, capacitors from Kemet [30] are selected based on the voltage and dv/dt rating requirements. For the experiment, components are chosen based on the available standard values. The device switching transients and load voltages are shown for *RC* and *RLC* filters in Fig. 13 and L_{aux}, *LR*, and *LRC* filters in Fig. 14, respectively.

A. Output L_{aux}

The output inductor is designed in order to move the antiresonance frequency of the cable and motor from 6.57 MHz to a lower frequency. In this case, the output inductor is designed such that the antiresonance frequency is shifted to 2.4 MHz, as shown in Fig. 12. This is done by sweeping a 20-dB/dec line from low frequency toward high frequencies such that the first resonant point in the impedance lies to the right. With the inductor, all the high-frequency antiresonances are not present anymore. The resonance around 16 MHz is because of the self-resonant frequency of the inductor. The output inductor helps reduce the switching losses by about 9.1% and reduces both turn-ON and turn-OFF times of the device. The dv/dt at the load is reduced by 68%. However, the output inductor reduces the reflected wave voltage at the load end to only 1.4 pu and increases the damping time of the reflected wave by 30%. To reduce the peak load voltage to 1.2 pu, a larger inductance has to be used. But, this would further increase the damping time, which would result in undesired increase in switching losses due to undamped reflected waves.

B. RC Filter

The *RC* filter is installed at the motor terminal to provide impedance between the cable and the motor. The resistance value is chosen to be close to the characteristic impedance of the cable. The capacitance required depends on the length of the cable and the overshoot voltage allowed for the given rise time of the pulse. It is given as

$$C = -\frac{3(l_c\sqrt{L_C C_C})}{2Z_0 ln(0.95)} = 7.6\ n\text{F}. \tag{7}$$

The resistance is chosen to be standard 100 Ω resistor, and a capacitance of 10 nF is chosen. From the impedance plot in Fig. 12, it can be seen that, with the *RC* filter, the first resonance

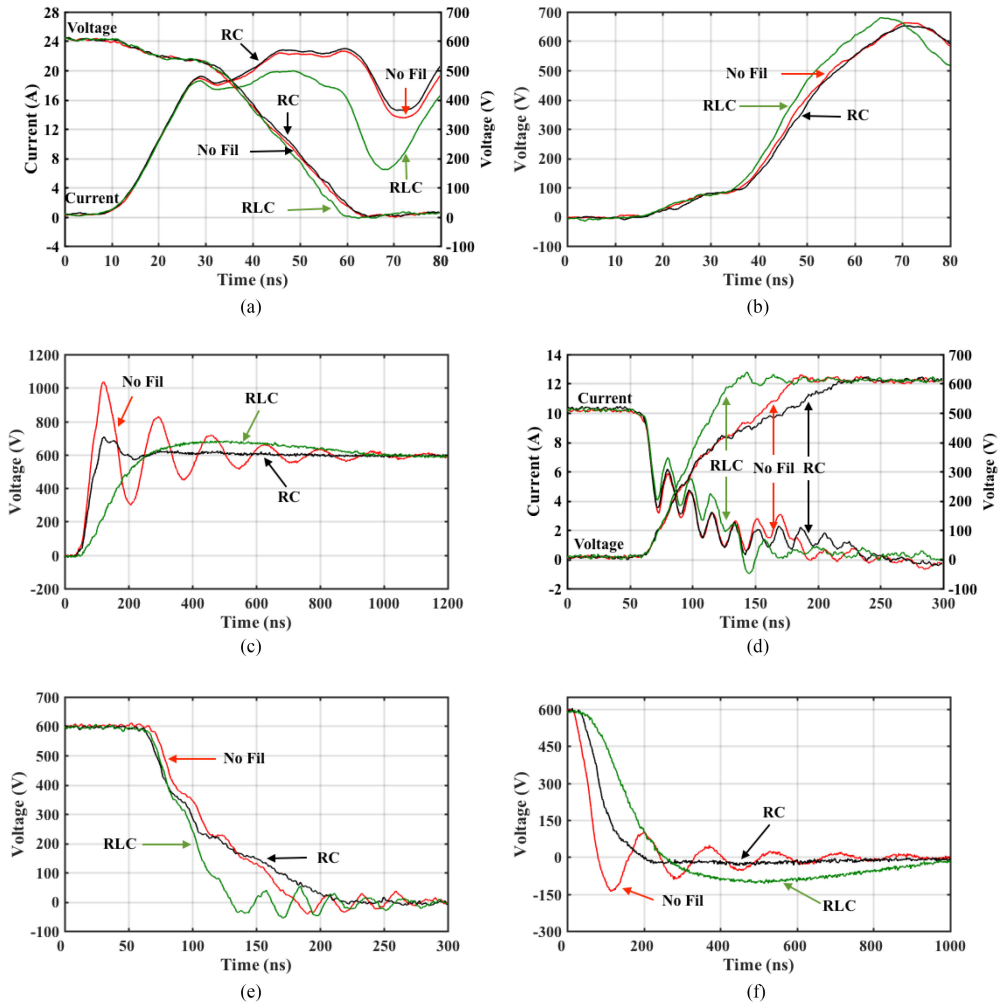

Fig. 13. Influence of *RC* and *RLC* Filters on Switching Characteristics. (a) ON-transient: V_{TL} & I_{TL}. (b) OFF-transient: V_{TL} & I_{TL}. (c) ON-transient: V_L. (d) OFF-transient: V_{TL} & I_{TL}. (e) OFF-transient: V_{TH}. (f) OFF-transient: V_L.

shifts from 230 to 65 kHz. The impedance becomes capacitive above 65 kHz till the second resonance frequency. Also, the location of resonances and antiresonance above 1 MHz do not change. Therefore, the *RC* filter does not help in the reduction of switching losses. Because the overall impedance has become more capacitive, the losses increase. From the Table VI, the switching losses increase by 4%, and the turn-ON and turn-OFF times also increases. The losses in the resistor are about 3.6 mJ, and the dv/dt at load reduces by 48% for a load voltage of 1.05 pu.

TABLE VII
INFLUENCE OF DIFFERENT OUTPUT FILTERS ON SWITCHING CHARACTERISTICS

Filter	E_{on} (μJ)	E_{off} (μJ)	E_{sw} (μJ)	E_{Filter} (mJ)	dv/dt (V/ns)	t_{damp} (ns)	V_{Load} pu	ΔE_{sw} %
None	288	108	396	-	15.8	766	1.7	-
RC	292	120	412	3.6	10.6	190	1.2	4.1
RLC	263	94	357	1.76	2.8	744	1.2	-9.6
LR	272	99	371	0.120	6.7	186	1.1	-6.2
L // RC	270	97	367	0.110	1.9	1360	1.1	-7.1
L	261	98	359	-	4.9	995	1.4	-9.1

C. RLC Filter

The *RLC* uses a combination of the output inductor and the *RC* filter at the output of the inverter. The *RC* network provides impedance matching, and the output inductor helps reduce the dv/dt of the output pulse. The following filter transfer function is solved to obtain *L* and *C* values:

$$H = \frac{1 + sRC}{1 + sRC + s^2LC}. \tag{8}$$

From the impedance plot in Fig. 12, it can be seen that the first resonance point is shifted from 230 to 100 kHz. However, because of the inductor, the high-frequency antiresonance are not present anymore. The resonance around 16 MHz is due to the self-resonant frequency of the output inductor. From Table VII, the filter losses are 1.76 mJ and a reduction in load dv/dt is about 82% for a load voltage of 1.2 pu.

D. LR Filter

The *LR* filter uses an output inductor in parallel with a resistor. The resistor is chosen to provide impedance matching with the

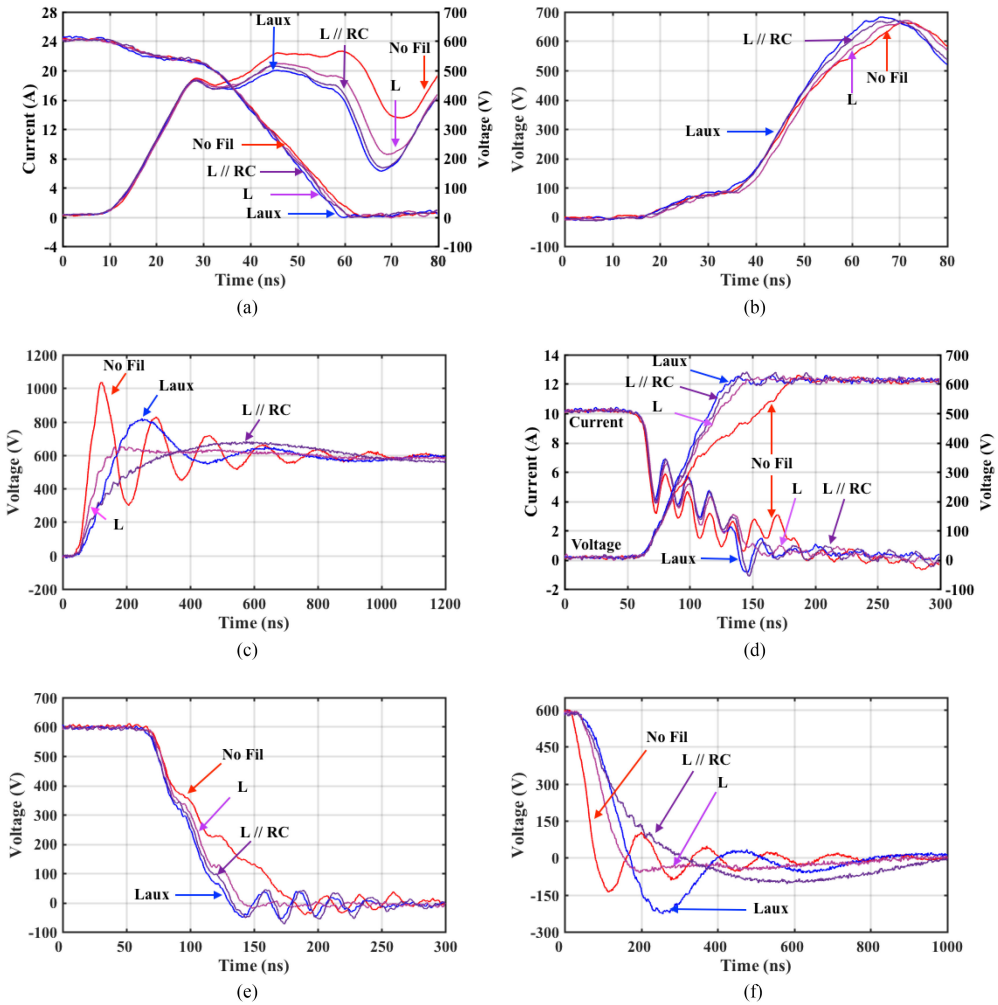

Fig. 14. Influence of L_{aux}, *LR*, and *L // RC* output filters on switching characteristics. (a) ON-transient: V_{TL} & I_{TL}. (b) OFF-transient: V_{TL} & I_{TL}. (c) ON-transient: V_L. (d) OFF-transient: V_{TL} & I_{TL}. (e) OFF-transient: V_{TH}. (f) OFF-transient: V_L.

filter. The value of *L* is dependent on the voltage overshoot and is given by the following equation:

$$L = -\frac{l_C L_C}{ln(2(1-\frac{1.2}{1+\Gamma_L}))} = -\frac{4\times 540\times 10^{-9}}{ln\left(2\left(1-\frac{1.2}{1+1.8}\right)\right)} = 5.4\ \mu\text{H}. \tag{9}$$

From the impedance plot in Fig. 12, the low-frequency resonance is unaffected but the high-frequency antiresonances that cause the losses are not present anymore. However, the impedance is still lower than L_{aux} or *RLC* filter. Therefore, the reduction in losses is about 6.2%, which are lower than L_{aux} or *RLC* filters. The losses in the filter are about 120 μJ and dv/dt at load reduces by 57% for a load voltage of 1.1 pu.

E. L//R Filter

The *L // RC* filter uses an output inductor in parallel with a *RC* network. The *RC* network is chosen such that the filter provides impedance matching to the cable while also reducing the filter losses. Condition for selection of *R* for given *L* is given by the following equation:

$$R \le \frac{\sqrt{(L+L_C)/(C_C)}}{2}. \tag{10}$$

From the impedance plot in Fig. 12, the low-frequency resonance is unaffected, but the high-frequency antiresonances that cause the losses are not present any more. However, the impedance is still lower than L_{aux} or *RLC* filter but higher than the *LR* filter. Therefore, the reduction in losses is about 7.1%, which is lower than L_{aux} or *RLC* filters and higher than *LR* filter. The losses in the filter are about 110 μJ, and dv/dt at load reduces by 88% for a load voltage of 1.1 pu. However, the damping time of the reflected wave voltage is higher than all filters and is about 1.36 μs.

F. Comparison of Different Filters

The test results are summarized in Table VII. The normalized values of dv/dt, t_{damp}, ΔEsw, and E_{losses} is shown in Fig. 15. It can be seen that the *L* filter and *RLC* filter have the highest reduction in switching losses. This is made possible by shifting

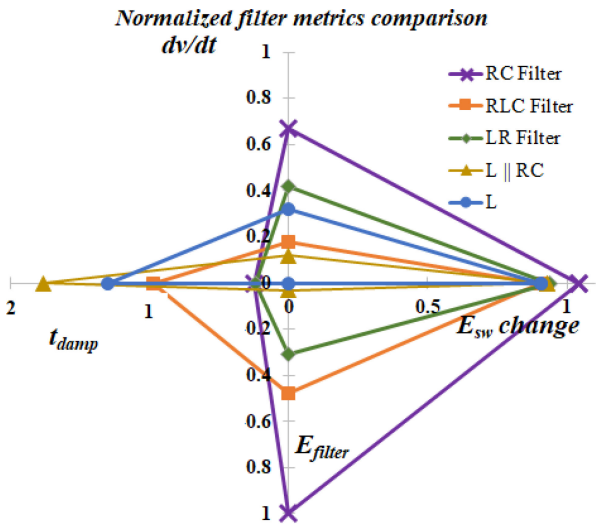

Fig. 15. Comparison of normalized switching loss reduction, filter loss, output dv/dt and damping time of reflected wave with different filters (E_{sw}, t_{damp}, and dv/dt normalized for case without filter and E_{loss} normalized for the *RC* filter losses).

the first antiresonance to lower frequencies while masking the antiresonances at higher frequencies. But, the *RLC* filter suffers from very high losses in the resistor, thus increasing the overall losses by four times the switching loss. The *L* filter only offers a moderate reduction in peak voltage while having a 30% increase in damping time. This makes it suitable only for low switching frequency applications and low cable length applications. Using the inductor at the output of the inverter helps decouple the high-frequency impedance seen by the inverter and therefore helps switching loss reduction. But, the damping time of the RW and magnitude of the RW increases. Therefore, this filter is suitable for low switching frequency applications. The *RC* filter has the highest filter losses in the filter and also increases the switching losses. Therefore, it is not desirable to use this filter. Similar to the *RC* filter, the *RLC* filter also suffers from high filter losses and does not offer better metrics when compared to the other filters. The conclusions drawn here are only for the case under study here. At higher power levels and different cable lengths, case-by-case study taking into account the conduction losses in the inductor is required in order to identify the optimum filter topology. Owing to the limitation of length of the article, this analysis will be part of future publication.

VII. Conclusion

This article revisits the reflected wave phenomenon with the focus on the influence of undamped reflected waves. This becomes essential with ever-increasing switching frequencies of inverters in motor drives due to the emergence of high-speed low inductance motors. The undamped reflected wave was seen to increase or decrease the switching loss depending on the whether the next pulse was applied during the peak or trough of the switching transient. The effects would be more pronounced, resulting in even greater changes in switching losses in high power drives due to higher damping times of the reflected wave. This article has presented a demonstration of this phenomenon and was limited by the available test setup. Both motor's and cable's antiresonance in the impedance affect the frequency of the reflected wave voltage and currents, which in turn are shown to affect the device switching losses. The effect of increasing cable lengths on the switching losses, turn-ON and turn-OFF times are presented. Different output filters are designed to mitigate the reflected wave and their impact on the switching characteristics is observed. A maximum reduction in switching losses was observed with the L_{aux} and *LRC* filter. This is because these filters effectively decouple the loads from the inverter. Other effects of employing an L_{aux} filter is the increased damping time of the reflected wave voltage and ineffective reduction of the peak magnitude of reflected wave voltage. While the *RLC* filter provides good reflected wave voltage suppression, it increases the overall system loss considerably. The *RC* terminal filter was found to be very lossy for reflected wave voltage suppression and also does not help reduce switching losses. Both *LR* and *L // RC* filters find the middle ground in switching loss reduction and the losses in the filter resistor. The *LR* filter has the lowest damping times, making it ideal for high switching frequency applications. Therefore, for WBG devices-based inverters operating at high switching frequencies, the *LR* filter makes the best candidate. The *L // RC* filter has high damping time while offering lowest dv/dt at the load. This makes it a good candidate for WBG inverters with low switching frequency applications such as retrofit drives where the motor may need a lower dv/dt.

Acknowledgment

The authors would like to thank A. Deshpande, A. I. Emon, and S. Rai for their support in discussion and experiments.

References

[1] R. J. Kerkman, D. Leggate, D. Schlegel, and G. Skibinski, "PWM inverters and their influence on motor overvoltage," in *Proc. APEC Conf. Twelfth Annu. Appl. Power Electron. Conf. Expo.*, vol. 1, Feb. 1997, pp. 103–113.

[2] D. Leggate, J. Pankau, D. W. Schlegel, R. J. Kerkman, and G. L. Skibinski, "Reflected waves and their associated current [in IGBT VSIs]," *IEEE Trans. Ind. Appl.*, vol. 35, no. 6, pp. 1383–1392, Nov. 1999.

[3] L. A. Saunders, G. L. Skibinski, S. T. Evon, and D. L. Kempkes, "Riding the reflected wave-IGBT drive technology demands new motor and cable considerations," in *Proc. Petroleum Chem. Ind. Conf., Rec. Conf. Papers. Inst. Elect. Electron. Eng. Incorporated Ind. Appl. Soc. 43rd Annu.*, Sep. 1996, pp. 75–84.

[4] A. F. Moreira, T. A. Lipo, G. Venkataramanan, and S. Bernet, "High-frequency modeling for cable and induction motor overvoltage studies in long cable drives," *IEEE Trans. Ind. Appl.*, vol. 38, no. 5, pp. 1297–1306, Sep. 2002.

[5] R. M. Tallam, G. L. Skibinski, T. A. Shudarek, and R. A. Lukaszewski, "Integrated differential-mode and common-mode filter to mitigate the effects of long motor leads on ac drives," *IEEE Trans. Ind. Appl.*, vol. 47, no. 5, pp. 2075–2083, Sep. 2011.

[6] D. A. Rendusara and P. N. Enjeti, "An improved inverter output filter configuration reduces common and differential modes dv/dt at the motor terminals in PWM drive systems," *IEEE Trans. Power Electron.*, vol. 13, no. 6, pp. 1135–1143, Nov. 1998.

[7] A. von Jouanne and P. N. Enjeti, "Design considerations for an inverter output filter to mitigate the effects of long motor leads in ASD applications," *IEEE Trans. Ind. Appl.*, vol. 33, no. 5, pp. 1138–1145, Sep. 1997.

[8] M. C. Sousounis, J. K. H. Shek, and M. A. Mueller, "Filter design for cable overvoltage and power loss minimization in a tidal energy system with onshore converters," *IEEE Trans. Sustain. Energy*, vol. 7, no. 1, pp. 400–408, Jan. 2016.

[9] M. M. Swamy and M. A. Baumgardner, "New normal mode dv/dt filter with a built-in resistor failure detection circuit," *IEEE Trans. Ind. Appl.*, vol. 53, no. 3, pp. 2149–2158, May/Jun. 2017.

[10] S. Lee and K. Nam, "Overvoltage suppression filter design methods based on voltage reflection theory," *IEEE Trans. Power Electron.*, vol. 19, no. 2, pp. 264–271, Mar. 2004.

[11] M. M. Swamy, J. K. Kang, and K. Shirabe, "Power loss, system efficiency, and leakage current comparison between Si IGBT VFD and SiC FET VFD with various filtering options," *IEEE Trans. Ind. Appl.*, vol. 51, no. 5, pp. 3858–3866, Sep. 2015.

[12] S. Yin, K. J. Tseng, R. Simanjorang, Y. Liu, and J. Pou, "A 50-kW high-frequency and high-efficiency SiC voltage source inverter for more electric aircraft," *IEEE Trans. Ind. Electron.*, vol. 64, no. 11, pp. 9124–9134, Nov. 2017.

[13] Z. Zhang, F. Wang, L. M. Tolbert, B. J. Blalock, and D. J. Costinett, "Evaluation of switching performance of SiC devices in PWM inverter-fed induction motor drives," *IEEE Trans. Power Electron.*, vol. 30, no. 10, pp. 5701–5711, Oct. 2015.

[14] I. Josifovi, J. Popovi-Gerber, and J. A. Ferreira, "Improving SiC JFET switching behavior under influence of circuit parasitics," *IEEE Trans. Power Electron.*, vol. 27, no. 8, pp. 3843–3854, Aug. 2012.

[15] S. Walder and X. Yuan, "Effect of load parasitics on the losses and ringing in high switching speed SiC MOSFET based power converters," in *Proc. IEEE Energy Convers. Congr. Expo.*, Sep. 2015, pp. 6161–6168.

[16] P. Yi, P. K. S. Murthy, and L. Wei, "Performance evaluation of SiC mosfets with long power cable and induction motor," in *Proc. IEEE Energy Convers. Congr. Expo.*, Sep. 2016, pp. 1–7.

[17] Z. Zhang, F. Wang, L. M. Tolbert, B. J. Blalock, and D. J. Costinett, "Decoupling of interaction between WBG converter and motor load for switching performance improvement," in *Proc. IEEE Appl. Power Electron. Conf. Expo.*, Mar. 2016, pp. 1569–1576.

[18] B. Narayanasamy, A. S. Sathyanarayanan, A. Deshpande, and F. Luo, "Analysis and mitigation of reflected wave voltages and currents in wbg devices based motor drives," in *Proc. IEEE 4th Workshop Wide Bandgap Power Devices Appl.*, Nov. 2016, pp. 297–301.

[19] B. Narayanasamy, A. S. Sathyanarayanan, A. Deshpande, and F. Luo, "Impact of cable and motor loads on wide bandgap device switching and reflected wave phenomenon in motor drives," in *Proc. IEEE Appl. Power Electron. Conf. Expo.*, Mar. 2017, pp. 931–937.

[20] M. Schinkel, S. Weber, S. Guttowski, W. John, and H. Reichl, "Efficient HF modeling and model parameterization of induction machines for time and frequency domain simulations," in *Proc. 21st Annu. IEEE Appl. Power Electron. Conf. Expo. APEC* , Mar. 2006, pp. 1181–1186.

[21] M. J. Scott *et al.*, "Reflected wave phenomenon in motor drive systems using wide bandgap devices," in *Proc. IEEE Workshop Wide Bandgap Power Devices Appl.*, Oct. 2014, pp. 164–168.

[22] R. M. Tallam and D. Leggate, "Control of a PWM voltage-source inverter in the pulse-dropping region to reduce reflected-wave motor overvoltage," *IEEE Trans. Ind. Appl.*, vol. 49, no. 2, pp. 873–879, Mar. 2013.

[23] H. Xiong, J. Zhang, and A. Von Jouanne, "Control of variable frequency drive PWM to mitigate motor overvoltage due to double pulsing in reflected wave phenomenon," in *Proc. IEEE Energy Convers. Congr. Expo.*, Sep. 2018, pp. 6563–6570.

[24] B. Mirafzal, G. L. Skibinski, and R. M. Tallam, "A failure mode for PWM inverter-fed ac motors due to the antiresonance phenomenon," *IEEE Trans. Ind. Appl.*, vol. 45, no. 5, pp. 1697–1705, Sep. 2009.

[25] Wolfspeed. MOSFET Evaluation Kit. [Online]. Available: https://www.wolfspeed.com/downloads/dl/file/id/1558/product/428/kit8020_crd_5ff0917p_2_application_note.pdf

[26] Lapp. Lapp olFlex 2XL VFD Cable Catalog. [Online]. Available: https://lappdigitallibrary.cld.bz/2016-LAPP-Catalog/94

[27] R. J. Kerkman, D. Leggate, and G. L. Skibinski, "Interaction of drive modulation and cable parameters on ac motor transients," *IEEE Trans. Ind. Appl.*, vol. 33, no. 3, pp. 722–731, May 1997.

[28] Ohmite. TGH Series Thick Film Power Resistors. [Online]. Available: https://www.ohmite.com/assets/docs/res_tgh.pdf?r=false

[29] Coilcraft. High Current Flat Wire Inductors. [Online]. Available: http://www.coilcraft.com/pdfs/ser1360.pdf

[30] Kemet. PHE450 Double Metallized Polypropylene Film. [Online]. Available: https://content.kemet.com/datasheets/KEM_F3033_PHE450.pdf

Balaji Narayanasamy (Student Member, IEEE) received the bachelor's degree in electrical and electronics engineering from Amrita University, Coimbatore, India, in 2012, and the master's degree in electrical engineering from the Ohio State University, Columbus, Ohio, USA, in 2016. He is currently working toward the Ph.D. degree in electrical engineering with the University of Arkansas, Fayetteville, AR, USA.

From 2012 to 2014, he worked as an Executive Engineer with L&T Kobelco Machinery, India. He has authored and coauthored twelve papers which were presented in different international conferences. His research interests include analysis and mitigation of EMI using high density passive and active EMI filters, and wide bandgap devices-based power converters.

Arvind Shanmuganathan Sathyanarayanan received the B.Tech in electrical and electronics engineering from VIT University, Vellore, India, in 2015, and the M.S. degree in electrical and computer engineering from the Ohio State University, Columbus, Ohio, USA, in 2017.

Since 2017, he has been working as Power Electronics Engineer with Safran Power, Twinsburg, OH, USA.

Fang Luo (Senior Member, IEEE) received the bachelor's and Ph.D. degrees in electrical engineering from the Huazhong University of Science and Technology,Wuhan, China, in 2003 and 2010, respectively.

From 2007 to 2010, he was a Joint Ph.D. Student with the Center for Power Electronics Systems (CPES), Virginia Tech, supported by the Chinese Scholarship Council and CPES. From 2010 to 2014, he was with CPES, Virginia Tech, as a Postdoctoral Researcher and also a Research Scientist. From 2014 to 2017, he was a Research Assistant Professor with the Ohio State University. In July 2017, he joined the University of Arkansas as a Tenure Track Assistant Professor. He is currently an Assistant Professor with the University of Arkansas, Fayetteville, AR, USA. His research interests include turbo-electric propulsion converters, high-power-density converter design, high-density electromagnetic interference filter design, and power module packaging/integration for wide-bandgap devices.

Cai Chen (Member, IEEE) received the B.S. degree and Ph.D. degree in electrical and electronic engineering from the Huazhong University of Science and Technology, Wuhan, China, in 2008 and 2014, respectively.

He is an Associate Research Fellow with Huazhong University of Science and Technology. From March 2013 to December 2013, he was an Intern in GE Global Research Center, Shanghai, China. From 2014 to 2016, he joined the Advanced Semiconductor, Packaging and Integration Lab, Huazhong University of Science and Technology, Wuhan, Hubei, China, as a Postdoctoral Researcher. From 2016 to 2017, he was a Visiting Scholar with the Center for High Performance Power Electronics, The Ohio State University, Columbus, OH, USA. From 2017 to 2018, he was a Visiting Scholar with the College of Engineering, University of Arkansas, Fayetteville, AR, USA. In 2019, he joined the Huazhong University of Science and Technology, Wuhan, China, as an Associate Research Fellow. His research interests include WBG devices packaging, integration, packaging EMI issues, packaging reliability, and high-density applications.